Fischer–Tropsch synthesis over CNT-supported cobalt catalyst: effect of magnetic field

Ali Nakhaei Pour, Javad Karimi, Sohrab Taghipoor, Mostafa Gholizadeh & Mohammadreza Hashemian

🖄 Springer

🖄 Springer

CrossMark

ORIGINAL PAPER

Fischer–Tropsch synthesis over CNT-supported cobalt catalyst: effect of magnetic field

Ali Nakhaei Pour[1] · Javad Karimi[2] · Sohrab Taghipoor[3] · Mostafa Gholizadeh[1] ·
Mohammadreza Hashemian[2]

Abstract In the present work, the cobalt catalysts supported on carbon nanotubes (CNTs) were prepared by impregnation method in the presence and absence of magnetic field. The prepared catalysts were employed to yield higher hydrocarbons via Fischer–Tropsch synthesis. It is explored that using magnetized water can effectively change the catalyst geometry in impregnation catalyst preparation method. For the preparation of different sizes of cobalt particles on the CNTs support, the physical properties of solvent (water) in impregnation process were changed using the magnetizing process. The results showed that the average particle sizes of impregnated cobalt nanoparticles were decreased by using magnetized water in impregnation step. In addition, in the magnetized treated cobalt catalyst, the cobalt particles mostly dispersed outside the tubes because the capillary forces decreased by reducing water surface tension. Furthermore, the experimental results showed that the probability of chain growth (α) and selectivity to heavier hydrocarbons increased in magnetized water treatment catalysts.

Keywords Fischer–Tropsch Synthesis · CNTs support · Impregnation method · Cobalt catalysts · Magnetized water

✉ Ali Nakhaei Pour
a.nakhaei@um.ac.ir; nakhaeipoura@yahoo.com

1 Department of Chemistry, Ferdowsi University of Mashhad, P.O. Box 9177948974, Mashhad, Iran

2 Research and Developed Center, Golriz Company, Toos Industrial Park, Mashhad, Iran

3 Research Institute of Petroleum Industry of National Iranian Oil Company, P.O. Box 137-14665, Tehran, Iran

Introduction

Fischer–Tropsch synthesis (FTS) offers a practical method in order of the production of higher hydrocarbons from syngas (a mixture of hydrogen and carbon monoxide). This process enables preparing high-quality hydrocarbon products without sulfur and other metals from coal or natural gas [1–3]. The FTS process was catalyzed by transition metals such as cobalt, iron, and ruthenium presenting the highest activity [4–6]. Among these transition metals, the cobalt catalysts were preferred due to some advantages like as: high activity in FTS process and low activity to water–gas shift (WGS) reaction, high selectivity to paraffinic hydrocarbons in products, high stability, and low cost in comparison with ruthenium [7, 8]. But, the reactivity of cobalt particles with oxidic support like as alumina and silica during the preparation of catalyst is a common drawback [9]. Formation of cobalt-support compounds reduced the activities of the prepared catalysts in FTS process [10–12].

Carbon nanotubes (CNTs) have quickly gained interest after the discovery in 1991 [13]. As a catalyst support, CNTs are inert and have a high chemical stability in aggressive media and are not able to interact strongly with metals [6, 14–17]. Nevertheless, it is possible to modify the surface in order to introduce anchoring sites for metals. When carbon materials are used as support in catalysis, the material is often pretreated with an oxidizing agent like concentrated nitric acid, removing impurities and introducing oxygen-containing groups as anchoring sites [18, 19]. The metal is often loaded on the support by impregnation with an aqueous metal precursor solution or by deposition precipitation [20, 21]. Magnetization of the solvent may change the solvent properties and affect the impregnation process [22]. Chang and Weng [23] and Hosoda et al.

⚫ Springer

[24] investigated the hydrogen bond strength enhancement over the magnetic fields caused by increasing electromagnetic attractions between the positive and negative poles of atoms in hydrogen bonds. Cai et al. [22] studied the treatment impact of the magnetization on water structure using H-NMR spectroscopy and concluded that larger size of water clusters was obtained by magnetization.

In the present work, the magnetic field effect is investigated in impregnation of mono-disperse cobalt nanoparticles on CNTs support. Magnetized water was used as a solvent for impregnation of cobalt on CNTs support. The Co/CNT catalysts with various sizes of particle were prepared by impregnation method using magnetized water, and the activities of prepared catalysts are evaluated in the Fischer–Tropsch synthesis.

Experimental

Magnetic-assisted precipitation process

Dynamic magnetization approach was implemented for magnetization of water. In this case, a magnetic treatment system was assembled as shown in Fig. 1. The deionized water was magnetized by passing into a coaxial static magnetic system with field strength of 6500G (AQUA CORRECT device). The certain volume of purified water in a close loop was circulated from closed tank linked to a pump of centrifugal used to circulate water in the system. The flow rate was settled at around 36 L min^{-1}. Previous studies show that properties of magnetized water remain constant for a long time. [25, 26].

Characterization of magnetized water

The capillary tube technique used to determine surface tension with four replications for each value [27]. Alternatively, since the surface tension is proportional to the capillary rise, the interest fluid is compared to a reference fluid of known surface tension. In this method, the surface tension is calculated using Eq. (1) and reported as a result.

$$\gamma = \frac{1}{2}\rho g r \left(h + \frac{r}{3} \right) \tag{1}$$

where r is the capillary radius (1 mm in our measurements), h is the capillary rise (m), g is the gravitational acceleration (9.8 m s^{-2}) and ρ is the liquid density (kg m^{-3}). Water
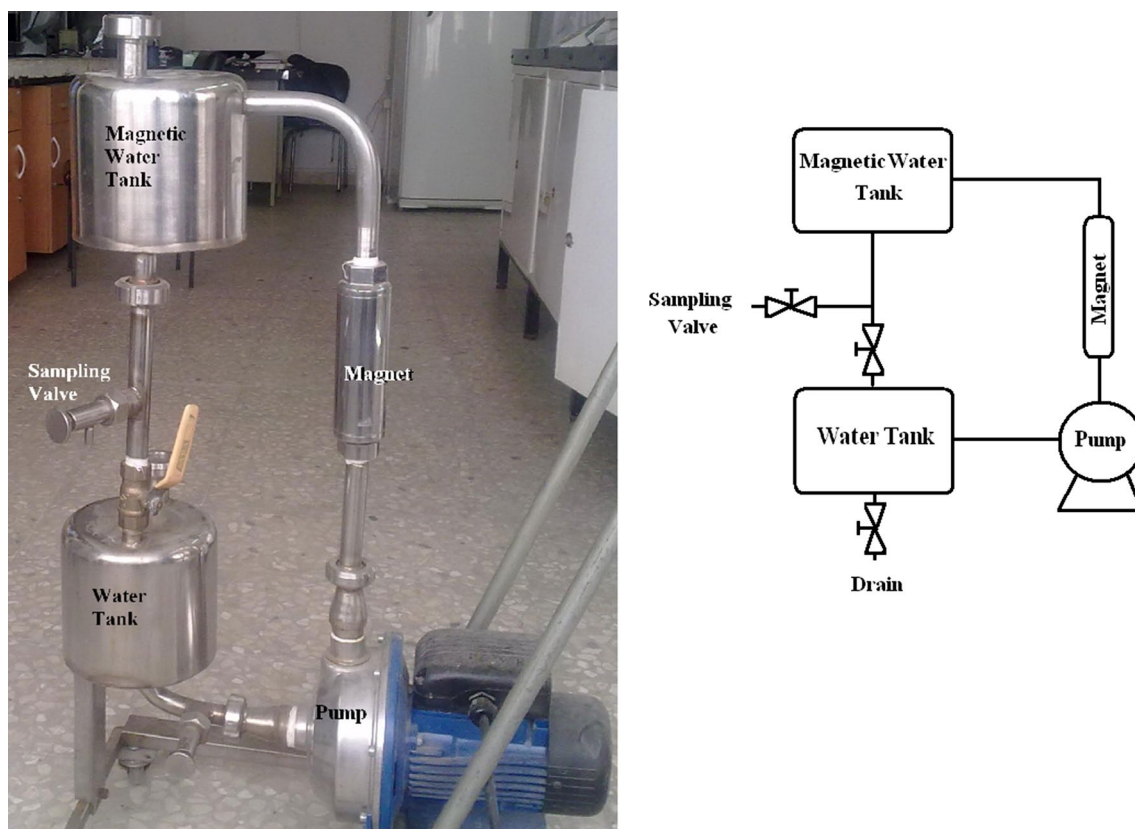
Fig. 1 Schematic magnetic treatment system

surface tension depends on temperature, so our measurements were carried out at impregnation temperature condition. For the measurement of the magnetized water surface tension, the samples were passed through strong magnetic field and measurements were taken quickly after the sample preparation. The measurements of the viscosity of magnetized water were carried out on a commercially available PHYSICA MCR300 (Paar Physica, Germany) with a double-gap cylinder (DG 26.7).

Catalyst preparation

The cobalt catalysts were prepared via incipient wetness impregnation method with 15 wt% cobalt loading on multiwall CNT support [6, 16, 28]. For the elimination of the amorphous carbons, the CNT support was purified by HNO_3 treatment process, dried at 120 °C for 8 h and calcined at 400 °C, before impregnation of cobalt. The catalysts were prepared using of cobalt nitrate [$Co(NO_3)_2 \cdot 6H_2O$ 99.0%, Merck] solution on CNT support. The catalyst precursors were dried overnight at 120 °C and calcined at 360 °C for 3.5 h.

To evaluate the effect of magnetization water in impregnation method, a series of catalysts were prepared with 0-, 5- and 10-pass water. The cobalt nitrate salts dissolved in the magnetized water and catalysts are marked as Co–CNT_0, Co–CNT_5 and Co–CNT_{10}.

Catalyst characterization

Nitrogen physisorption of the calcined catalysts was measured with an ASAP-2010 Micrometrics system to obtain the BET specific surface area, pore volume, and pore size distribution. All the samples were degassed at 200 °C for 4 h under 50 mTorr vacuums, before the physisorption measurement. Pore volume and pore diameter of the samples are calculated from adsorption and desorption isotherms at a relative pressure (P/P_0) of 0.98.

After calcination, the measurements of the XRD on fresh catalysts were conducted using an X-ray diffractometer with Cu/Kα radiation (Philips PW1840). The average size of cobalt oxide crystallites (d_{XRD}) was calculated using Scherrer equation for the Co_3O_4 peak located at $2\theta = 36.9°$ which is related to (311) plane and $K\psi$ factor of 0.89. The size of Co_3O_4 particle was converted to the corresponding cobalt metal particle size (dCo^0) according to the relative molar volumes of metallic cobalt and Co_3O_4, as Eq. (2):

$$d\left(Co^0\right)(nm) = 0.75 \times d(Co_3O_4)(nm) \qquad (2)$$

Temperature-programmed reduction (TPR) spectra of the fresh catalysts were obtained using a Micromeritics TPD–TPR Model 2900, which was equipped with thermal conductivity detector (TCD). To remove the traces of water, the catalyst samples were purged in argon flow at 300 °C and were cooled to 50 °C before reduction. The samples were heated from 50 to 825 °C with a ramp of 10 °C min^{-1}. A hydrogen–argon mixture (5.1% V_{H_2}/V_{Ar}) with the flow rate of 40 N mL min^{-1} was used for the reduction of catalysts.

The X-ray photoelectron spectroscopy (XPS) spectra were recorded to detect the nature of cobalt nanoparticles in the prepared samples after the calcination by a PHI-5800 Physical Electronics spectrometer using a monochromatized Al Kα source (1486.6 eV). The C1s line (284.6 eV) was consider as a reference for the correction of the electrostatic charging.

The hydrogen chemisorptions were done using the Micromeritics (TPD–TPR 2900 system). About 0.2 g of each catalyst was reduced at 365 °C for 12 h. Then, the sample degassed under argon flow at 100 °C in order to remove the weakly adsorbed hydrogen for 30 min. The result of temperature-programmed desorption (TPD) was obtained by increasing the temperature of the samples to 400 °C under the flow of the argon gas with a ramp rate of 10 °C min^{-1}. The results of the H_2-TPD were used to determine the cobalt dispersion and the average surface particle size. In calculation of catalyst dispersion, it was assumed that one hydrogen molecule covered two cobalt surface atoms. The dispersion of the catalysts was attained by the following formula:

$$D(\%) = \frac{\text{Number of } Co^0 \text{ atom on surface}}{\text{Number of Co atoms in sample}} \times 100 \qquad (3)$$

For the calculation of cobalt particle size, we assumed spherical uniform cobalt metal particles with a site density of 14.6 at.nm^{-2} [29]. These assumptions lead to the following formula:

$$D(\%) = 96/d\left(Co^0\right)(nm) \qquad (4)$$

where D denotes the dispersion and dCo^0 is the metallic cobalt particle diameter.

The morphology of the cobalt catalysts was observed with a LEO 912 AB transmission electron microscope instrument (Germany). The average particle size (d_{TEM}) and particle size distribution of cobalt nanoparticles located on and into of CNTs tubes were calculated via counting more than 100 particles in each TEM images.

Catalyst activity

The FTS activity based on produced hydrocarbons (HC) per catalyst weight (mol HC g_{cat}^{-1} h^{-1}) and products selectivity (based on carbon balance) for each catalyst were

evaluated using tubular fixed bed stainless steel reactor. The micro-reactor was placed in a special molten salt bath for temperature uniformity within the reactor, and the temperature of the batch was controlled via PID temperature controller. Separated Brooks's 5850 mass flow controllers were used to control H_2 and CO flow rates at desired rates.

About 1 g of each calcined cobalt catalysts was charged into the reactor. Before testing, the catalysts were reduced in situ at 400 °C for 12 h under a stream of H_2 at 1 bar and space velocity of 60 N mL min^{-1}. After reduction, the FTS reactions were carried out at 220 °C, 20 bar, $H_2/CO = 2$ and 40 N mL min^{-1}, feed rate.

The hydrocarbon products were analyzed using a set of three gas chromatographs (GC) for analyzing of hydrogen, LPG, unconverted feed and heavy hydrocarbons. The selectivity of products and feed conversion were calculated based on the GC analyses results and carbon balance in the range of 97 and 103%.

Results and discussion

Effects of magnetic field on physical properties of water

The influence of the magnetic field on water surface tension is presented in Fig. 2. The surface tension of water (calculated by using Eq. 1) over number of passes through the magnetic field (Fig. 2) was measured to show the change in behavior of water molecules by a external magnetic field. The results of Fig. 2 showed that increasing the number of passes through the magnetic field with 6500 Gauss strength leads to the decrease in the surface tension of the water solution. The surface tension of the distilled water after more than eight passes reached to a constant value. It was included that after more than eight passes, decreasing surface tension of distilled water was not significant, and it was not significantly higher with more passes. As shown in Fig. 2, the surface tension of distilled water after ten passes decreased about 21% [30].

Due to the polarity of water molecule, its behavior and motion will be affected by the magnetic field. The viscosity of water was measured over treatment pass through the magnetic field (result indicated in Fig. 3). Figure 3 shows that whether the behavior of water changed by a magnetic field, it was shown more than 10% increase after 10 passes through 6500 Gauss strength.

Morphologies of the activated CNTs

Table 1 summarizes the textural properties of the fresh and acid-treated carbon nanotubes. These data (Table 1) indicated that the surface area, total pore volume, and
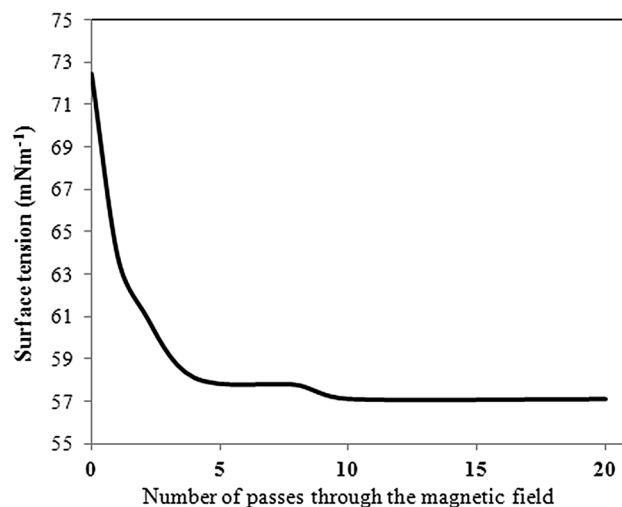
Fig. 2 Influence of the magnetic field and number of passes through the magnetic field on the surface tension of the distilled water
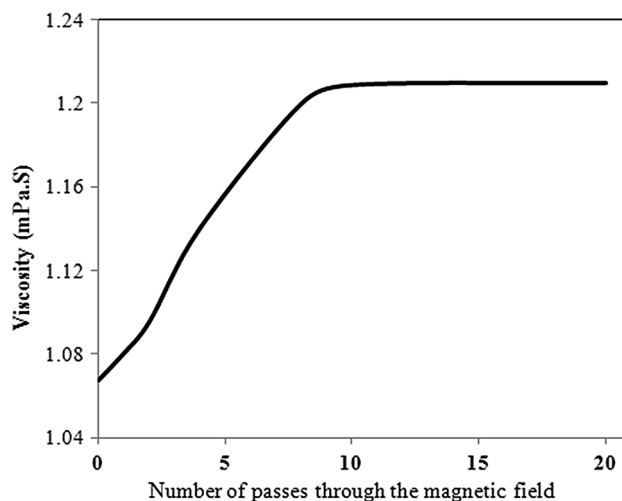

Fig. 3 Influence of the magnetic field and number of passes through the magnetic field on the viscosity of the distilled water

average internal diameter of nanotubes increased significantly in acid-treated CNTs support. These conditions resulted in better dispersion of metal as well as catalyst activity enhancement. As shown in Table 1, the total amount of metals decreased to zero in acid-treated CNTs.

Figure 4 shows the liquid N_2 adsorption isotherms of activated CNTs. The rapid increase for nitrogen absorbed below $P/P_0 = 0.05$ by the activated CNTs suggests the presence of abundant micro-pores. In addition, a slow uptake of N_2 was observed at the intermediate P/P_0, which indicated the adsorption of N_2 on the external surfaces of the activated CNTs. The form of

Table 1 Textural properties of the support

| Sample	BET surface area (m^2/g)	Total pore volume (mL/g)	Average pore diameter (Å)	% metals
Fresh CNTs	209	0.5	91.6	0.6
30% HNO_3 Treated CNTs	252	0.6	94.1	0.0
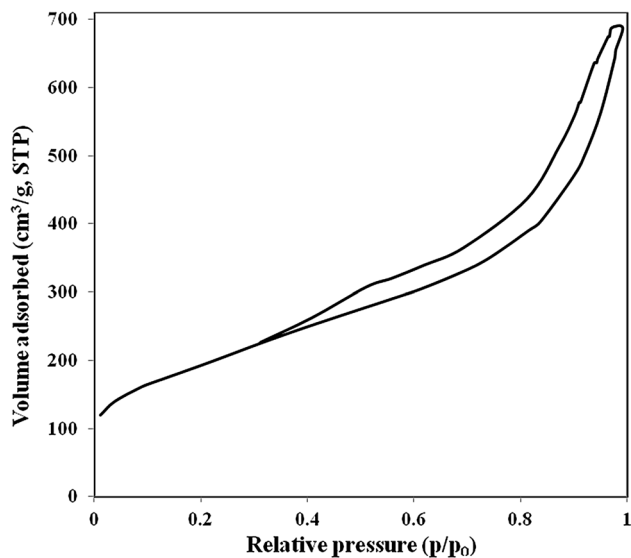
Fig. 4 Liquid N_2 adsorption–desorption isotherm of the activated CNTs

hysteresis loop (in the N_2 isotherms) in the high P/P_0 range indicates that the activation of CNTs support had produced mesopores and opened the caps of the CNT tubes.

One of the important parameters for porous materials is the pore size distribution (PSD). To obtain PSD of the purified CNTs, BJH method (for 2–50 nm regions) used from the isotherm of adsorption branch, and the results are shown in Fig. 5. The PSD of the purified CNTs shows three main peaks in the micro-pore region at 2–4 nm and mesoporous region at 7–10 and 15–25 nm. Thus, the purified CNTs were rich in micro-pores and mesopores.

Catalyst characterization results

Figure 6 shows the X-ray diffraction patterns (XRD) of the fresh catalysts after calcination. In Fig. 6, the peaks which are located at 2θ values of 25° and 43° were related to the CNT support, and the other peaks were related to different crystal planes of Co_3O_4 [14, 31]. As shown in Fig. 6, the peak which was located at 2θ value of 36.8° is the strongest one of the Co_3O_4 in the XRD spectra of all catalysts which
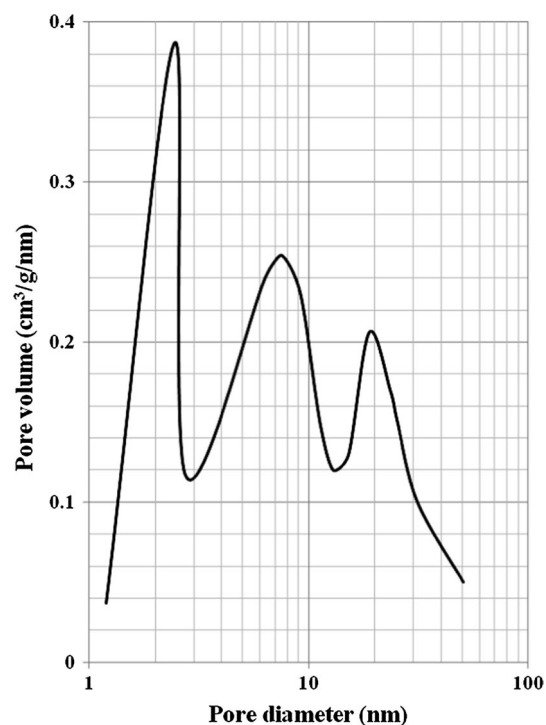
Fig. 5 Pore size distribution (PSD) of the purified CNTs from the adsorption branch of the isotherm
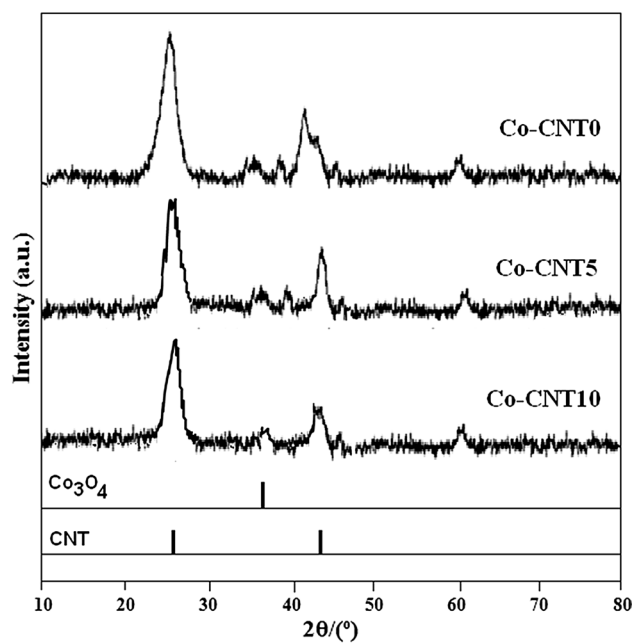
Fig. 6 X-ray diffraction patterns of the calcined catalysts

correspond to the (311) plane. Also, minor peaks observed at 44° (400), 59° (511) and 65° (440) correlate with a cubic spinel structure of Co_3O_4 based on JCPD: 78-1970 for all the catalysts [32]. The XRD results showed that using the

magnetized water in impregnation step does not change the crystal structure of Co_3O_4. Note that the XRD pattern peaks in magnetized water are much broader than non-treatment system, which are related to lower cobalt particle sizes.

Table 2 shows the average Co_3O_4 crystallite sizes of catalysts, which were calculated from XRD spectra after calcination (using the Scherer equation at 2θ value of 36.8°). The results were determined for the Co–CNT$_0$, Co–CNT$_5$, Co–CNT$_{10}$ as approximately 16.1, 14.2 and 12.5 nm, corresponding to 12.1, 10.7, 9.4 nm of cobalt metal sizes, respectively.

The TEM images and calculated particle size distribution of the cobalt in prepared catalysts are shown in Fig. 7. These TEM images reveal the dispersion of the cobalt particles inside and outside the CNTs channels. These results show that the narrow interior width of the CNTs tubes controlled the introduction of particles in sizes close to the channels diameter (10 nm), and all particles of sizes about 10 nm and higher are lying on the external surface of the CNTs channels [33, 34]. The inside cobalt particles were produced due to capillary force in impregnation process, which led to incarceration of cobalt particles within the CNTs channels [35, 36]. In the case of Co–CNT$_5$ and Co–CNT$_{10}$ catalysts, the cobalt particles dispersed mostly on the outside the CNTs tubes and the fraction of the particles lying at the outer surface of the CNTs support are higher than the Co–CNT$_0$ catalyst. In capillary impregnation, the driving force is the capillary pressure that depends on solution surface tension and characteristic pore size [37, 38]. Thus, the capillary forces decreased by reducing the water surface tension, and we expected that the particles lying at the inner of the CNTs support were decreased in magnetized water-prepared catalysts (Co–CNT$_5$ and Co–CNT$_{10}$). TEM images (Fig. 7) show the fraction of particles inside/outside the tubes were 49, 43 and 37%, for Co–CNT$_0$, Co–CNT$_5$, and Co–CNT$_{10}$ catalysts, respectively.

Figure 7 shows that the cobalt nanoparticle size distributions decreased for magnetized treated water. Lower surface tension of the magnetized water decreased the critical size of nucleus and increased the rate of nucleation in nucleation process, which leads to a higher number of particles [39]. Moreover, higher viscosity of the solvent in the magnetized water system decreased the mass transport process, so the growth of particles in precipitation process

is decreased. As a result, the prepared solids in magnetized water have smaller particle diameter than the bulk. As shown in Fig. 7, the magnetized water controls the cobalt distribution in a narrow size. According to Fig. 7, the average particle sizes for Co–CNT$_0$, Co–CNT$_5$, and Co–CNT$_{10}$ catalysts are about 12.4, 11.2 and 9.8 nm, respectively.

The reducibility of the prepared cobalt catalysts in H_2 atmosphere was determined by TPR experiments, which are shown in Fig. 8. The low temperature peak (300–400 °C) is in general assign to reduction of Co_3O_4 to CoO [8, 11, 14, 40].

$$Co_3O_4 + H_2 \rightarrow 3CoO + H_2O \qquad (5)$$
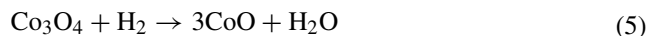
The second wide-ranging peak is corresponding to reduction of little CoO to Co^0 species.

$$3CoO + 3H_2 \rightarrow 3Co + 3H_2O \qquad (6)$$
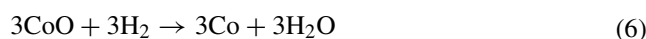
The amount of hydrogen necessary for the two-step formation of one mol metallic cobalt is 1/3 mol in the first step and 1 mol in the second step with respect to the amount of cobalt, while a portion of the first peak in TPR spectrum may comprise the reduction of the CoO species on the surface of the catalysts to metallic Co and/or the reduction of cobalt species that interact with the support. The area under the second reduction peak (Fig. 8) of the samples TPR patterns is three times of the first reduction peak area. Therefore, the cobalt crystalline phase mostly contains Co_3O_4 species in three prepared catalysts. According to Fig. 8, Co–CNT$_5$ and Co–CNT$_{10}$ catalysts have shifted the reduction peaks to a higher temperature compared to the Co–CNT$_0$ catalyst. The cobalt oxide nanoparticles in Co–CNT$_0$ catalyst are easily reduced due to the confinement of cobalt particles inside the tubes [19, 33]. Reduction of cobalt oxide nanoparticles encapsulated in CNTs was facilitated in comparison with the species out of CNTs, due to the surface electron deficiency of inside of CNTs tubes [41, 42].

XPS technique was used to identify the nature of cobalt nanoparticles in the calcined catalysts. The XPS spectra of the cobalt catalysts, which focus on Co2p region, are shown in Fig. 9. As reported in the previous section, cobalt crystalline phase for our prepared catalysts is mostly Co_3O_4. Cobalt exhibits two oxidation states in Co_3O_4 spinel structure, two Co^{3+} in octahedral symmetry (with higher

Table 2 H_2 uptake, dispersion (%) and average Co particle size of the catalysts

Catalyst	H2 uptake (μmole H$_2$ desorbed/g$_{cat}$)	Dispersion (%)		dp Co (nm)		
		XRD results	H$_2$ TPD	XRD results	TEM average	H2 TPD
Co–CNT$_0$	104	7.9	8.2	12.1	12.4	11.7
Co–CNT$_5$	124	9.0	9.3	10.7	11.2	10.9
Co–CNT$_{10}$	143	10.2	10.8	9.4	9.8	9.6

Fig. 7 TEM images of the calcined catalysts. **a** Co–CNT$_{10}$; **b** Co–CNT$_5$; **c** Co–CNT$_0$
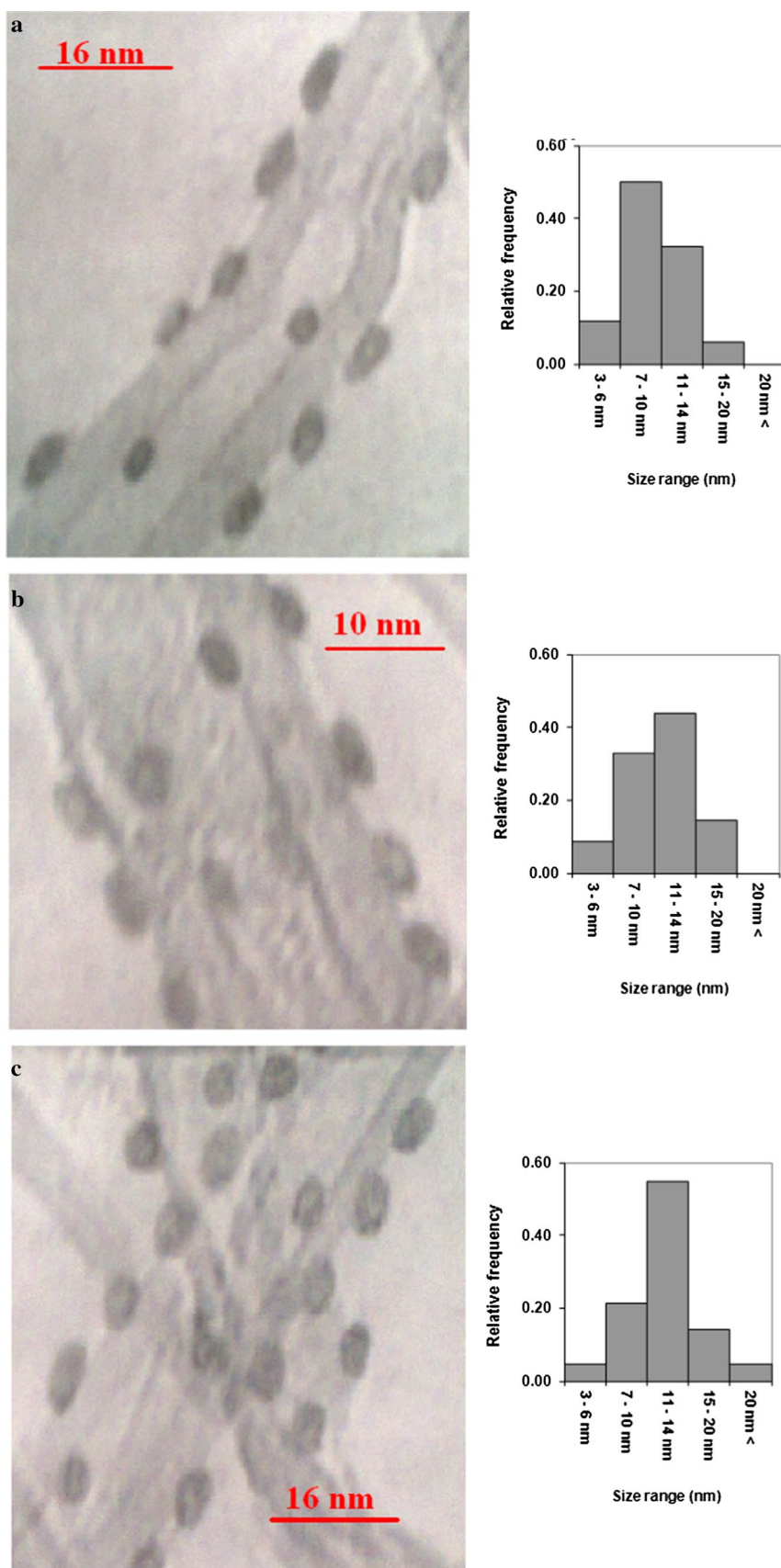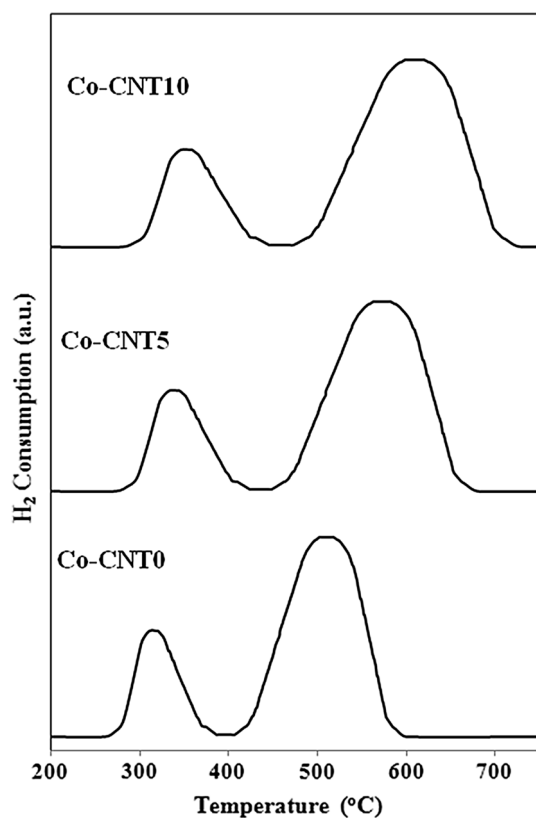
Fig. 8 TPR patterns of the calcined catalysts

Fig. 9 Co2p XPS spectra of catalyst samples

binding energy in XPS spectra) and one Co^{2+} in tetrahedral symmetry. Thus, an asymmetric shape of the cobalt $2p_{3/2}$ peak is observed in Fig. 9 [33, 43, 44]. The XPS spectrum of the catalysts shows two essentially peaks at binding energies of 781 eV for 2p3/2 and 796 eV for 2p1/2. The shoulders that are appeared at around 789 eV for $2p_{3/2}$ and at 805 eV for $2p_{1/2}$ may be related to unexpected defeat. Because of interaction of CNTs support with cobalt particles, the effect of the CNTs C1s peak at the 285.2 eV must be considered to reimburse for charging and work function effects.

According to Fig. 9, the location of the key peak in the Co2p XPS spectrum for all catalysts is shifted to a higher binding energy, due to the presence of CoO with Co_3O_4 main phase. The ratio of intensity of Co2p1/2 shoulder to its main peak was used to make a difference between the cubic CoO and the spinel Co_3O_4. This ratio is about 0.9 for CoO and ~0.3 for Co_3O_4 [45]. This ratio is about 0.3, 0.42 and 0.48 for Co–CNT$_0$, Co–CNT$_5$ and Co–CNT$_{10}$, respectively. Thus, we concluded that there is the presence of CoO in magnetized water-prepared catalysts. The hydrogen chemisorption on the reduced cobalt catalysts was used to determine cobalt dispersion, and the cobalt particle size was estimated. For this purpose, we assumed that the hydrogen atoms were adsorbed as H/Co atomic

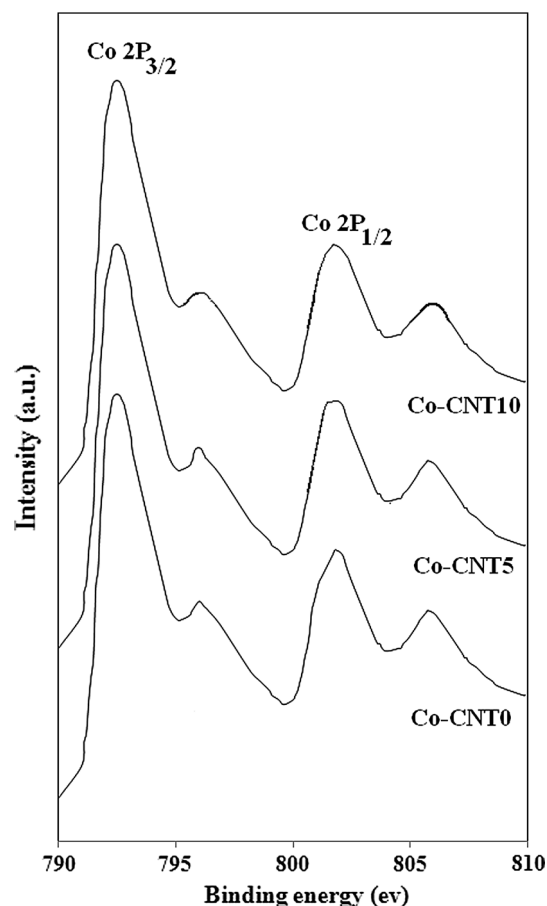ratio [46]. The results of the hydrogen chemisorption of the catalysts are represented in Table 2. As shown in Table 2, with decreasing the cobalt particle size, the H_2 desorption improved from 104 to 143 µmol /g$_{cat}$. Bezemer et al. [47] observed that H_2 desorption is changed with cobalt particle size (for particles <10 nm), but this trend levels-off bigger particles. Table 2 shows that the average size of the cobalt metal particle varied from 9.6 to 11.7 nm, and cobalt dispersion changed from 8.2 to 10.8 (%); these data are in good agreement with XRD and TEM results.

Fischer–Tropsch synthesis

Figure 10 shows the relative results of FTS reaction rate (Mol HC produced/g$_{cat}$/min) after 25–30 h on stream for prepared catalysts. It exposed that catalysts prepared through the magnetized water display a higher FTS rate than non-treatment catalysts. The cobalt active sites produced by magnetized water are more stable than ones produced by non-treatment water, because of their uniformity [48]. These results expose that the FTS activity of the

catalysts depends on the uniformity and size distribution of the cobalt clusters [5, 15, 28, 49]. Thus, higher surface-to-volume ratio of catalysts with smaller cobalt particle size leads to higher cobalt–time yield.

The number of CO molecules converted per active site per second or turnover frequencies (TOF) is defined as the site–time yields. The site–time yields (TOF) in our calculations were calculated by using the number of active sites obtained from TEM results for prepared catalysts. Figure 11 shows the site–time yields calculated after 25–30 h on stream. Although the FTS reaction rate (mol HC $g^{-1}_{cat}.h^{-1}$) increased substantially from Co–CNT$_0$ to Co–CNT$_{10}$, the site–time yields decreased (from 35.6 to 30.3×10^{-3} s^{-1}) when the cobalt particle size becomes smaller. In addition, the previous results show that the exterior surfaces of the CNTs tubes are electron rich and the internal ones are electron poor [13, 36, 50]. Due to

low electron density inside CNTs surface, the nanoparticles confinement within the CNT tubes gives electron to the inside CNTs surface, which profits the dissociative adsorption of CO molecules on the cobalt surfaces [33, 50]. Thus, each cobalt catalytic site that is placed within the CNTs tubes has to be more active than the one on the external surface. As mentioned, non-treatment water increased the cobalt particles located within the CNTs tubes. In addition, another reason for TOF enhancement in Co–CNT$_0$ catalyst is the high active cobalt particles within the CNTs tubes.

Table 3 lists the relative results of carbon monoxide conversion (%), selectivity to higher hydrocarbons and chain growth probability calculated after 25–30 h time-on-stream for all catalysts. This table shows that CO conversion (%) increased from 75% for the Co–CNT$_0$ to 84% for the Co–CNT$_{10}$ catalysts. This table predicts

Fig. 10 Relationship between the catalyst and FTS rate (g HC produced/g$_{cat}$/h) calculated after 25–30 h on stream. FTS condition: $T = 220$ °C, $P = 20$ bar, H$_2$/CO = 2.0, and GHSV = 40 N mL/(g$_{cat}$ h)
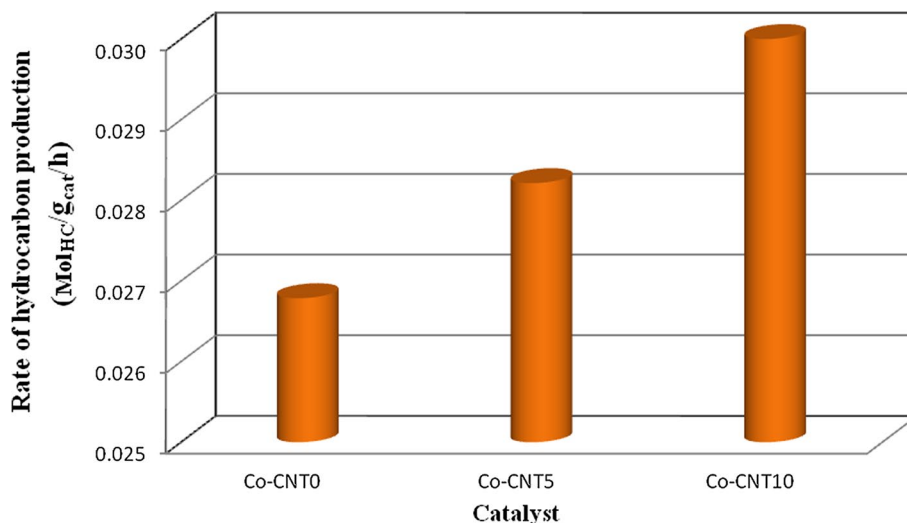

Fig. 11 Cobalt–time yields calculated after 25–30 h on stream [$T = 220$ °C, $P = 20$ bar, H$_2$/CO = 2.0, and GHSV = 40 N mL/(g$_{cat}$ h)]
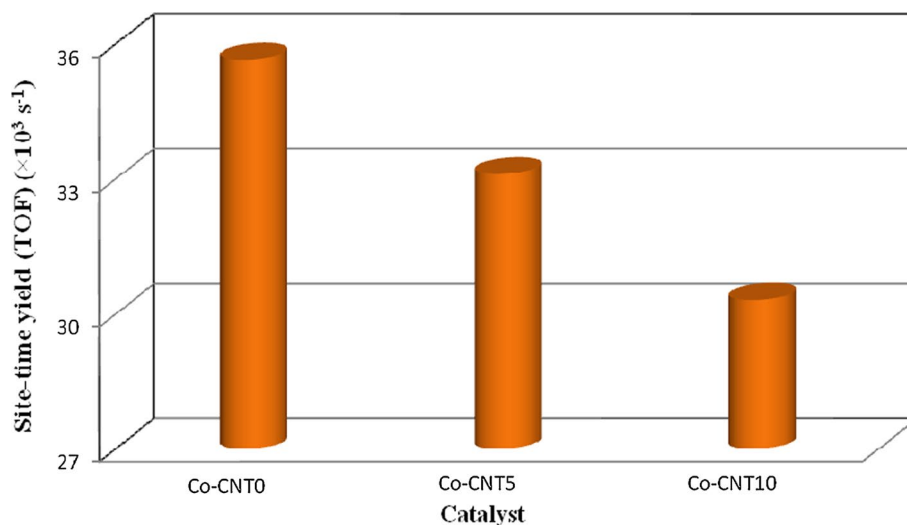
that the cobalt particle size restricted the catalyst activity (as %CO conversion in Table 3). Furthermore, this table shows that the chain growth probability and higher hydrocarbons selectivity increased in magnetized water treatment catalysts. Figure 12 represents the connection between the cobalt catalysts preparation methods and produced hydrocarbons distributions after 20–25 h time-on-stream.

These data confirm the results of Bezemer et al. [47] and Borg et al. studies [51]. Bezemer et al. [47] found that the C_{5+} selectivity depends on cobalt particle size, only for particles size with dimensions between 3 and 8 nm for carbon supported catalysts. Borg et al. [49] reported that the C_{5+} selectivity depends on cobalt particle size, only for particles size larger than 10 nm, in alumina-supported cobalt catalysts. Here, in our study for CNT-supported cobalt catalysts prepared by modified impregnation method, the selectivity of C_{5+} hydrocarbons depends on cobalt particle size, only for particles size smaller than 10 nm. Differences in selectivity of C_{5+} hydrocarbons for our results in comparison with Borg et al. [49] possibly correlated with different support effects. The thin internal diameter of the CNTs channels (between 8 and 10 nm) controlled the incorporation of cobalt particles in sizes which is close to the channel diameter (10 nm). Thus, a lot of cobalt particles with diameter smaller than 10 nm may be placed within the tubes. In addition, lower surface tension of magnetized treated water reduced the capillary forces. TEM results showed that the particles lying at the inner of the CNTs support decreased in magnetized water-prepared catalysts (Co–CNT$_5$ and Co–CNT$_{10}$). The cobalt particles of the CNTs which are located inside the hollow tubes have different behavior due to limitation in hydrocarbons chain growth and diffusion effects. It seems that for non-treatment catalyst (Co–CNT$_0$) (with higher cobalt clusters lies in inner of CNTs tubes) the steric hindrance inhibited the growing higher chain hydrocarbons. Furthermore, chain growth probabilities and selectivity to higher hydrocarbons in the present prepared cobalt catalyst are strongly dependent on the particles imprisonment within CNTs tubes. Thus, the particles confinement within CNTs is more important than the particles size effects.
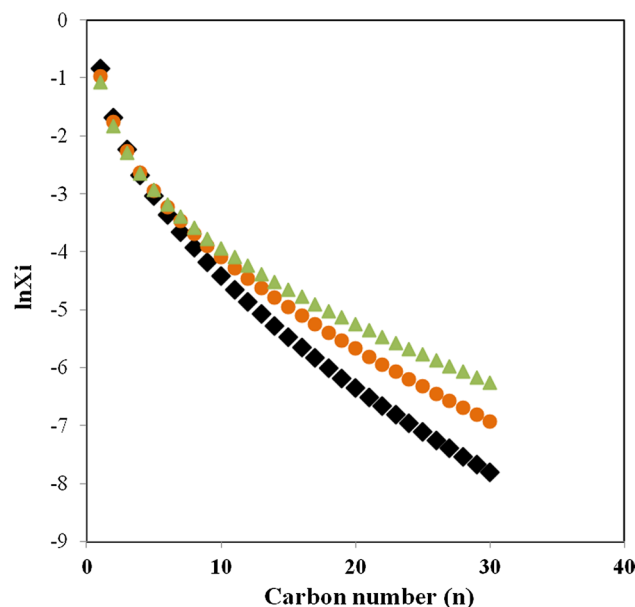
Fig. 12 Relationship between the catalysts and carbon number distribution of hydrocarbons formed calculated after 25–30 h, on stream (*filled square* Co–CNT$_{10}$; *filled circle* Co–CNT$_5$; *filled triangle* Co–CNT$_0$) FTS reaction condition: T = 220 °C, P = 20 bar, H$_2$/CO = 2.0, and GHSV = 40 N mL/(g$_{cat}$ h)

Conclusions

This study was attempted to prepare the CNTs-supported cobalt catalysts by a novel modified impregnation method using magnetized water. The prepared catalysts were employed to yield higher hydrocarbons in carbon monoxide hydrogenation (FTS) reaction. Cobalt nanoparticles were prepared by impregnation in the presence and absence of magnetic field. Our results have shown that the surface tension of distilled water which is used in impregnation step of cobalt nanoparticles decreases under the influence of a magnetic field. The surface tension of the water solvent was decreased from 72.5 to 51.1 (mNm^{-1}) after 10 passes through a magnetic field with 6500 Gauss strength. The results show that the average particle size of impregnated cobalt nanoparticles decreased by decreasing the surface tension of the water solvent in impregnation step. TPR results show that the cobalt crystalline phase mostly contains Co$_3$O$_4$ species, but XPS results show the presence

Table 3 CO conversion, chain growth probability and hydrocarbons selectivity % calculated after 25–30 h on stream [T = 220 °C, P = 20 bar, H$_2$/CO = 2.0, and GHSV = 40 N mL/(g$_{cat}$ h)]

Catalyst	CO conversion (%)	α	Selectivity (%)				
			CH$_4$	C$_2$–C$_4$	C$_5$–C$_{12}$	C$_{13}$–C$_{19}$	C$_{20+}$
Co–CNT$_0$	75	0.84	13.1	29.5	37.8	12.4	7.3
Co–CNT$_5$	79	0.90	9.2	23.1	38.1	17.0	12.5
Co–CNT$_{10}$	84	0.93	7.1	18.9	36.0	19.8	18.1

of minor of the CoO phase in three prepared catalysts. In the magnetized treated catalysts, the cobalt particles dispersed mostly outside the tubes because the capillary forces decreased by reducing of water surface tension. Furthermore, results showed that the chain growth probability (α) and selectivity to C_{5+} hydrocarbons increased in magnetized water treatment catalysts.

It seems that in catalyst prepared in non-treatment water, higher cobalt loaded in inner of CNTs tubes and the steric hindrance inhibited the growing higher chain hydrocarbons. Furthermore, chain growth probabilities and selectivity to higher hydrocarbons in the present prepared cobalt catalyst were strongly dependent on the particle's confinement within CNTs.

References

1. G.P. Van Der Laan, A.A.C.M. Beenackers, Kinetics and selectivity of the Fischer–Tropsch synthesis: a literature review. Catal. Rev. **41**, 255–318 (1999)
2. A. Nakhaei Pour, M.R. Housaindokht, J. Zarkesh, M. Irani, E.G. Babakhani, Kinetics study of CO hydrogenation on a precipitated iron catalyst. J. Ind. Eng. Chem. **18**, 597–603 (2012)
3. A.Nakhaei Pour, H. Khodabandeh, M. Izadyar, M.R. Housaindokht, Mechanistic double ASF product distribution study of Fischer–Tropsch synthesis on precipitated iron catalyst. J. Nat. Gas Sci. Eng. **15**, 53–58 (2013)
4. M.E. Dry, Fischer Tropsch Technology in *Studies in Surface Science and Catalysis*, ed. by S. André, D. Mark (Elsevier, Amsterdam, 2004), pp. 533–600
5. W. Ma, G. Jacobs, D.E. Sparks, M.K. Gnanamani, V.R.R. Pendyala, C.H. Yen et al., Fischer–Tropsch synthesis: support and cobalt cluster size effects on kinetics over Co/Al$_2$O$_3$ and Co/SiO$_2$ catalysts. Fuel **90**, 756–765 (2011)
6. A.Nakhaei Pour, M. Housaindokht, Fischer–Tropsch synthesis over CNT supported cobalt catalysts: role of metal nanoparticle size on catalyst activity and products selectivity. Catal. Lett. **143**, 1328–1338 (2013)
7. A.Y. Khodakov, W. Chu, P. Fongarland, Advances in the development of novel cobalt Fischer–Tropsch catalysts for synthesis of long-chain hydrocarbons and clean fuels. Chem. Rev. **107**, 1692–1744 (2007)
8. E. Iglesia, Design, synthesis, and use of cobalt-based Fischer–Tropsch synthesis catalysts. Appl. Catal. A **161**, 59–78 (1997)
9. A. Tavasoli, A.Nakhaei Pour, M.G. Ahangari, Kinetics and product distribution studies on ruthenium-promoted cobalt/alumina Fischer–Tropsch synthesis catalyst. J. Nat. Gas Chem. **19**, 653–659 (2010)
10. D. Schanke, A. Hilmen, E. Bergene, K. Kinnari, E. Rytter, E. Ådnanes et al., Study of the deactivation mechanism of Al$_2$O$_3$-supported cobalt Fischer–Tropsch catalysts. Catal. Lett. **34**, 269–284 (1995)
11. W. Chu, P.A. Chernavskii, L. Gengembre, G.A. Pankina, P. Fongarland, A.Y. Khodakov, Cobalt species in promoted cobalt alumina-supported Fischer–Tropsch catalysts. J. Catal. **252**, 215–230 (2007)
12. A. Karimi, A.Nakhaei Pour, F. Torabi, B. Hatami, A. Tavasoli, M.R. Alaei et al., Fischer–Tropsch synthesis over ruthenium-promoted Co/Al$_2$O$_3$ catalyst with different reduction procedures. J. Nat. Gas Chem. **19**, 503–508 (2010)
13. H. Dai, Carbon nanotubes: opportunities and challenges. Surf. Sci. **500**, 218–241 (2002)
14. A. Tavasoli, K. Sadagiani, F. Khorashe, A.A. Seifkordi, A.A. Rohani, A.Nakhaei Pour, Cobalt supported on carbon nanotubes—a promising novel Fischer–Tropsch synthesis catalyst. Fuel Process. Technol. **89**, 491–498 (2008)
15. A.Nakhaei Pour, E. Hosaini, A. Tavasoli, A. Behroozsarand, F. Dolati, Intrinsic kinetics of Fischer–Tropsch synthesis over Co/CNTs catalyst: effects of metallic cobalt particle size. J. Nat. Gas Sci. Eng. **21**, 772–778 (2014)
16. A.Nakhaei Pour, S.A. Taheri, S. Anahid, B. Hatami, A. Tavasoli, Deactivation studies of Co/CNTs catalyst in Fischer–Tropsch synthesis. J. Nat. Gas Sci. Eng. **18**, 104–111 (2014)
17. A.Nakhaei Pour, E. Hosaini, M. Izadyar, M.R. Housaindokht, Particle size effects in Fischer–Tropsch synthesis by Co catalyst supported on carbon nanotubes. Chin. J. Catal. **36**, 1372–1378 (2015)
18. M.N. Tchoul, W.T. Ford, G. Lolli, D.E. Resasco, S. Arepalli, Effect of mild nitric acid oxidation on dispersibility, size, and structure of single-walled carbon nanotubes. Chem. Mater. **19**, 5765–5772 (2007)
19. A. Karimi, B. Nasernejad, A.M. Rashidi, A. Tavasoli, M. Pourkhalil, Functional group effect on carbon nanotube (CNT)-supported cobalt catalysts in Fischer–Tropsch synthesis activity, selectivity and stability. Fuel **117**, 1045–1051 (2014)
20. A.J. Van Dillen, R.J. Terörde, D.J. Lensveld, J.W. Geus, K.P. De Jong, Synthesis of supported catalysts by impregnation and drying using aqueous chelated metal complexes. J. Catal. **216**, 257–264 (2003)
21. F. Pinna, Supported metal catalysts preparation. Catal. Today **41**, 129–137 (1998)
22. R. Cai, H. Yang, J. He, W. Zhu, The effects of magnetic fields on water molecular hydrogen bonds. J. Mol. Struct. **938**, 15–19 (2009)
23. K.-T. Chang, C.-I. Weng, The effect of an external magnetic field on the structure of liquid water using molecular dynamics simulation. J. Appl. Phys. **100**, 043917 (2006)
24. H. Hosoda, H. Mori, N. Sogoshi, A. Nagasawa, S. Nakabayashi, Refractive indices of water and aqueous electrolyte solutions under high magnetic fields. J. Phys. Chem. A **108**, 1461–1464 (2004)
25. B. Bazubandi, E. Moaseri, M. Baniadam, M. Maghrebi, M. Gholizadeh, Fabrication of multi-walled carbon nanotube thin films via electrophoretic deposition process: effect of water magnetization on deposition efficiency. Appl. Phys. A **120**, 495–502 (2015)
26. M.H.R. Mohassel, A. Aliverdi, R. Ghorbani, Effects of a magnetic field and adjuvant in the efficacy of cycloxydim and clodinafop-propargyl on the control of wild oat (*Avena fatua*). Weed Biol. Manag. **9**, 300–306 (2009)
27. J. Vanhanen, A.-P. Hyvärinen, T. Anttila, T. Raatikainen, Y. Viisanen, H. Lihavainen, Ternary solution of sodium chloride, succinic acid and water; surface tension and its influence on cloud droplet activation. Atmos. Chem. Phys. **8**, 4595–4604 (2008)
28. A.Nakhaei Pour, E. Hosaini, M. Feyzi, Prediction of cobalt particle size during catalyst deactivation in Fischer–Tropsch synthesis. J. Iran. Chem. Soc. **13**, 139–147 (2016)
29. Ø. Borg, S. Eri, E.A. Blekkan, S. Storsæter, H. Wigum, E. Rytter et al., Fischer–Tropsch synthesis over γ-alumina-supported cobalt catalysts: effect of support variables. J. Catal. **248**, 89–100 (2007)
30. Y.I. Cho, S.-H. Lee, Reduction in the surface tension of water due to physical water treatment for fouling control in heat exchangers. Int. Commun. Heat Mass Transf. **32**, 1–9 (2005)
31. M. Trépanier, A.K. Dalai, N. Abatzoglou, Synthesis of CNT-supported cobalt nanoparticle catalysts using a microemulsion

technique: role of nanoparticle size on reducibility, activity and selectivity in Fischer–Tropsch reactions. Appl. Catal. A **374**, 79–86 (2010)

32. M. Chougule, S. Pawar, P. Godse, R. Sakhare, S. Sen, V. Patil, Sol–gel derived Co3O4 thin films: effect of annealing on structural, morphological and optoelectronic properties. J. Mater. Sci. Mater. Electron. **23**, 772–778 (2012)

33. M. Davari, S. Karimi, A. Tavasoli, A. Karimi, Enhancement of activity, selectivity and stability of CNTs-supported cobalt catalyst in Fischer–Tropsch via CNTs functionalization. Appl. Catal. A **485**, 133–142 (2014)

34. D.Tasis, N. Tagmatarchis, A. Bianco, M. Prato, Chemistry of carbon nanotubes, Chemical reviews, **106**, 1105–1136 (2006)

35. J.-P. Tessonnier, O. Ersen, G. Weinberg, C. Pham-Huu, D.S. Su, R. Schlogl, Selective deposition of metal nanoparticles inside or outside multiwalled carbon nanotubes. ACS Nano **3**, 2081–2089 (2009)

36. P. Serp, E. Castillejos, Catalysis in carbon nanotubes. ChemCatChem **2**, 41–47 (2010)

37. R. Maatman, C. Prater, Adsorption and exclusion in impregnation of porous catalytic supports. Ind. Eng. Chem. **49**, 253–257 (1957)

38. A.Nakhaei Pour, M. Housaindokht, H. Monhemi, Effect of solvent surface tension on the radius of hematite nanoparticles. Colloid J. **76**, 782–787 (2014)

39. B. Billia, R. Trivedi, D. Hurle, *Handbook of Crystal Growth*, vol. 1B (North-Holland, Amsterdam, 1993)

40. G.L. Bezemer, A. van Laak, A.J. van Dillen, K.P. de Jong, Cobalt supported on carbon nanofibers—a promising novel Fischer–Tropsch catalyst, in *Studies in Surface Science and Catalysis*, ed. by B. Xinhe, X. Yide (Elsevier, Amsterdam, 2004), pp. 259–264

41. W. Chen, X. Pan, X. Bao, Tuning of redox properties of iron and iron oxides via encapsulation within carbon nanotubes. J. Am. Chem. Soc. **129**, 7421–7426 (2007)

42. W. Chen, Z. Fan, X. Pan, X. Bao, Effect of confinement in carbon nanotubes on the activity of Fischer–Tropsch iron catalyst. J. Am. Chem. Soc. **130**, 9414–9419 (2008)

43. I. Alstrup, I. Chorkendorff, R. Candia, B.S. Clausen, H. Topsøe, A combined X-ray photoelectron and Mössbauer emission spectroscopy study of the state of cobalt in sulfided, supported, and unsupported Co–Mo catalysts. J. Catal. **77**, 397–409 (1982)

44. A.Y. Khodakov, A. Griboval-Constant, R. Bechara, V.L. Zholobenko, Pore size effects in Fischer–Tropsch synthesis over cobalt-supported mesoporous silicas. J. Catal. **206**, 230–241 (2002)

45. Y. Yang, L. Jia, B. Hou, D. Li, J. Wang, Y. Sun, The correlation of interfacial interaction and catalytic performance of N-doped mesoporous carbon supported cobalt nanoparticles for Fischer–Tropsch synthesis. J. Phys. Chem. C **118**, 268–277 (2013)

46. J. Xiong, Ø. Borg, E.A. Blekkan, A. Holmen, Hydrogen chemisorption on rhenium-promoted γ-alumina supported cobalt catalysts. Catal. Commun. **9**, 2327–2330 (2008)

47. G.L. Bezemer, J.H. Bitter, H.P.C.E. Kuipers, H. Oosterbeek, J.E. Holewijn, X. Xu et al., Cobalt particle size effects in the Fischer–Tropsch reaction studied with carbon nanofiber supported catalysts. J. Am. Chem. Soc. **128**, 3956–3964 (2006)

48. H. Hayashi, L.Z. Chen, T. Tago, M. Kishida, K. Wakabayashi, Catalytic properties of Fe/SiO2 catalysts prepared using microemulsion for CO hydrogenation. Appl. Catal. A **231**, 81–89 (2002)

49. Ø. Borg, P.D.C. Dietzel, A.I. Spjelkavik, E.Z. Tveten, J.C. Walmsley, S. Diplas et al., Fischer–Tropsch synthesis: cobalt particle size and support effects on intrinsic activity and product distribution. J. Catal. **259**, 161–164 (2008)

50. M. Trépanier, A. Tavasoli, A.K. Dalai, N. Abatzoglou, Fischer–Tropsch synthesis over carbon nanotubes supported cobalt catalysts in a fixed bed reactor: influence of acid treatment. Fuel Process. Technol. **90**, 367–374 (2009)

51. Ø. Borg, N. Hammer, S. Eri, O.A. Lindvåg, R. Myrstad, E.A. Blekkan et al., Fischer–Tropsch synthesis over un-promoted and Re-promoted γ-Al2O3 supported cobalt catalysts with different pore sizes. Catal. Today **142**, 70–77 (2009)